Hindawi
International Journal of Aerospace Engineering
Volume 2019, Article ID 2064131, 10 pages
https://doi.org/10.1155/2019/2064131

Research Article

Design and Modeling of a Novel Transformable Land/Air Robot

He Wang[1], **Jiadong Shi**[1,2], **Jianzhong Wang**[1], **Hongfeng Wang**[1], **Yiming Feng**[1] and **Yu You**[1]

[1]*School of Mechatronical Engineering, Beijing Institute of Technology, Beijing 100081, China*
[2]*Key Laboratory of Biomimetic Robots and Systems, Ministry of Education, Beijing Institute of Technology, Beijing 100081, China*

Correspondence should be addressed to Jianzhong Wang; cwjzwang@bit.edu.cn

Received 14 May 2018; Revised 14 November 2018; Accepted 2 December 2018; Published 4 February 2019

Academic Editor: Seid H. Pourtakdoust

This paper describes a novel transformable land/air robot that is capable of terrestrial locomotion and aerial locomotion. What is unusual about the robot is that it can transform between the two modes of locomotion at will through the transformable mechanism, allowing the robot to overcome large obstacles in their mission environment. The wheel mechanism of the robot is shared by both terrestrial and aerial locomotion, instead of simply adding a quadrotor to a wheeled mobile robot. The objective of this paper is to design the robot and establish the kinematic and dynamic models for the transformable process. Herein, we focus on the design of the driving wheels and transformable mechanism. A series of experiments about the energy analysis and the transformation from aerial locomotion mode to terrestrial locomotion mode were performed with the physical prototype; the experiment results confirmed the validity of our design and the theoretical analysis that are helpful to optimize the key parameters in our design. Moreover, our work can provide a reference for the study of the flying car.

1. Introduction

The ability to explore areas that are risky and inaccessible to humans and easily deal with the complex terrains makes quadrotors an excellent choice in applications such as search and military surveillance [1, 2]. However, it is difficult for quadrotors to operate for an extended period of time and range because of their high-energy consumption [3, 4]; as we all know, terrestrial locomotion is more energy efficient. For these reasons, a robot that is capable of terrestrial and aerial locomotion can be better adapt to different environments at the same time can extend the operation time and range.

There have been many successful attempts to create robots with terrestrial and aerial locomotion capabilities, and many approaches to combining aerial locomotion and terrestrial locomotion have been proposed [5, 6]. However, in order not to affect the operating capabilities of each mode of locomotion and the overall mobility of the robot, the two modes of locomotion should share part of their structure or actuators that can avoid the increasing weight and design complexity of the robot [7–10]. The HyTAQ connects a cylindrical cage to a quadrotor through two revolute joints, allowing the cage to roll freely with respect to the main quadrotor body. Moreover, the flight control system and commands used for aerial locomotion can be used to control the terrestrial locomotion. Compared to the aerial mode, there is no need to overcome the weight of the robot in the terrestrial mode, and therefore the robot reduces the power consumption [11–13]. Recently, some robots share part of their structure or actuators by undergoing a transformation when changing the modes or adjusting its shape by itself to adapt to the mode of locomotion. The robot [14–16] is a two-wheeled terrestrial locomotion robot that transforms into a helicopter. In the terrestrial locomotion mode, the rotors and stabilizer bar used for aerial locomotion are folded down along the length of the robot's body. It transforms into its aerial locomotion mode by positioning itself on-end, with its long axis oriented vertically rather than horizontally, and unfolding its flight mechanisms. The rotors are attached to the rotor heads close to the drive shafts by passive hinges and thus unfold as the shafts begin to spin. Moreover, the researchers of the Deployable Air-Land Exploration Robot

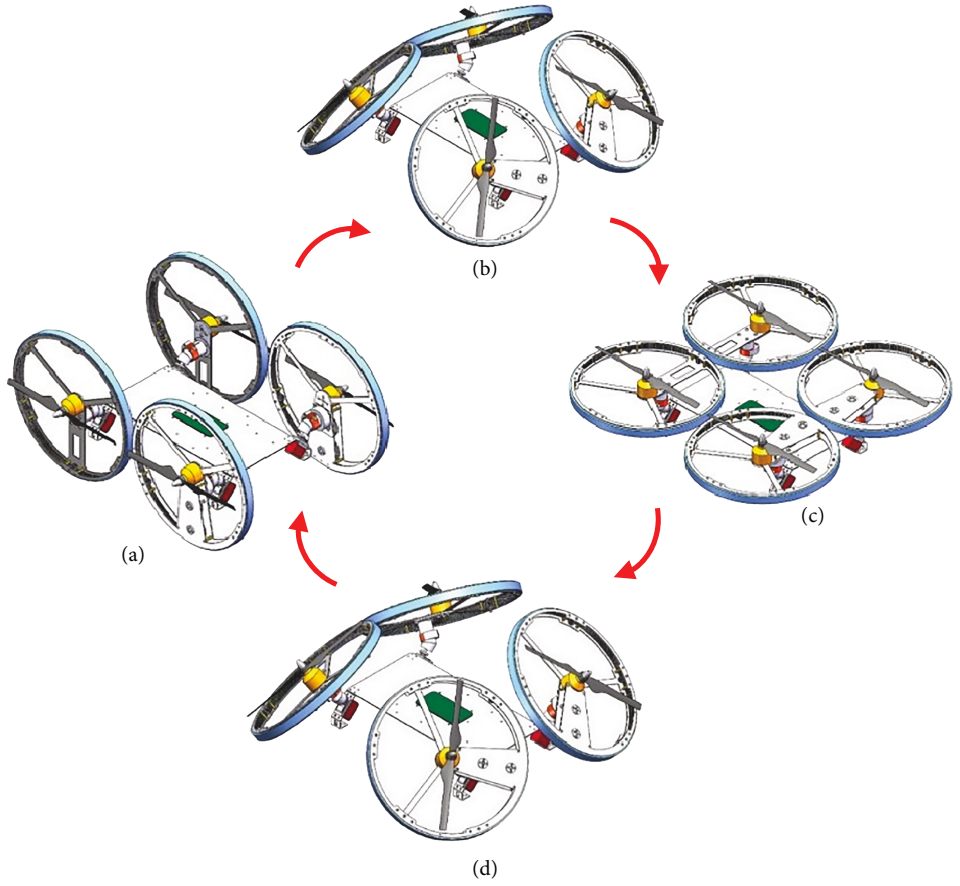

Figure 1: The full sequence of motions.

(DALER) propose a new approach, which is called "adaptive morphology", where parts of the structure of the robot are shared between the different modes of locomotion, instead of simply adding a second locomotion structure to an existing robot. It uses its wings as whegs to move on the ground, and the structure could self-adjust the shape to adapt to the locomotion mode. The efficiency of locomotion in each mode of locomotion can be improved through adaptive morphology suitable for that mode [17, 18].

Inspired by these works, we introduce a novel transformable land/air robot that is capable of terrestrial locomotion and aerial locomotion and enables to transform between the two modes of locomotion at will. It combines wheels with quadrotor, and the wheels are shared by both aerial and terrestrial locomotion, instead of simply adding a quadrotor to a wheeled mobile robot, and therefore avoid increasing weight and design complexity of the robot. The robot is primarily used on the ground, the intent of the aerial locomotion mode is to deal with the large obstacles, across complex terrain. Firstly, we described the outline of the platform's structure, and detailed the design of the driving wheels and transformable mechanism. Secondly, we established the kinematic and dynamic models for the transformable process. Then the transformation and energy analysis experiments were performed with the physical prototype. Finally, conclusions are drawn in Section 5.

2. Design of the Novel Transformable Land/Air Robot

There are three states of the robot in the process of motions. The full sequence is illustrated in Figure 1, (a) represents the state of terrestrial locomotion, (b) and (d) represent the state of a transformable process between the two modes of locomotion, respectively, and (c) represents the state of aerial locomotion.

2.1. Design of the Platform. The robot consists of three parts: running part, mode transformation part, and flying part. The running part realizes the stable running on the ground by adopting the architecture of two-wheel differential drive. The flying part realizes the stable flight by quadrotor mechanism. The mode transformation between the two modes of locomotion is directly driven by servos. Figure 2 shows the configuration of the platform.

The control system of the robot is shown in Figure 3. The communication between an operator and the robot is conducted wirelessly. The running part and mode transformation part are controlled by a microcontroller (STM 32F407); the flying part is controlled by the APM2.8. The APM2.8 is composed of MCU and IMU which can provide the raw data of flight attitude and velocity, and the APM2.8 is mainly used for flight attitude control and navigation.

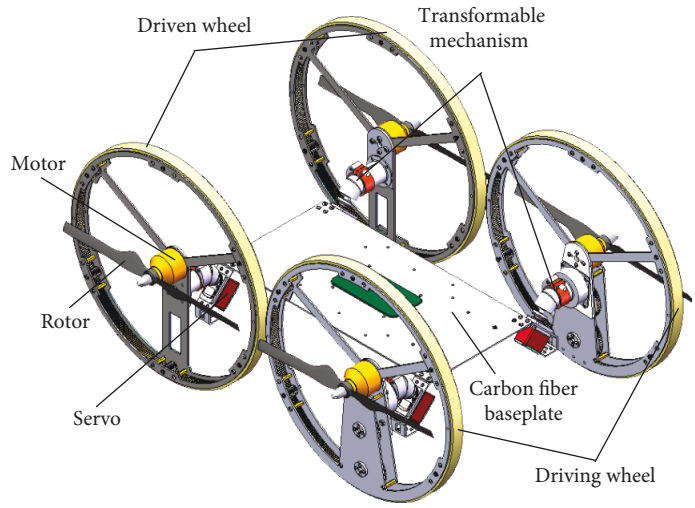

Figure 2: Configuration of the platform.

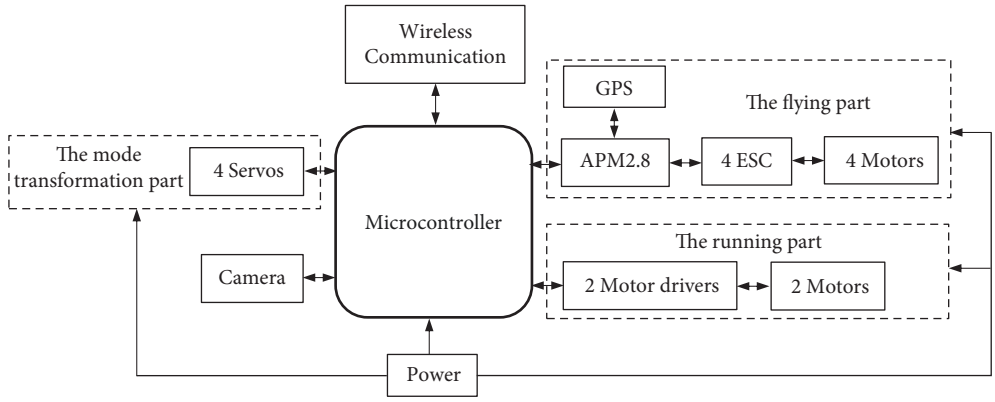

Figure 3: The control system of the transformable land/air robot.

The external GPS module can provide position information for the APM2.8. A Li-PO battery is used as the power supply. A microvideo camera mounted on the baseplate is equipped to take clear pictures and send to the control terminal real time.

2.2. Driving Wheel. The design of the driving wheel is very crucial. Figure 4 shows the whole structure of the driving wheel. In the terrestrial locomotion mode, the carbon fiber brackets on both sides of the wheel do not rotate. The motor for running drives the gear train and further drives the gear ring to complete the terrestrial locomotion. Gear train and gear ring play an important role in reducing speed and increasing torque while transmitting motion. The external diameter of the gear ring is slightly larger than the rotors, allowing the wheels to protect the rotors from obstacles such as rubble and wall. The 0.5 mm gap between gear ring and carbon fiber bracket ensures the gear ring rotate smoothly. The carbon fiber brackets on both sides of the wheel are connected and supported through plastic studs, and its external diameter is slightly smaller than the gear ring, ensuring itself do not contact the ground. The gears at the edge of the wheels support and mesh with the gear ring to make the gear ring rotate smoother.

In aerial locomotion mode, the wheels are the mounting seat of the motor for flying. The rotors and its driving motors are installed at the center of the wheels, and they are cross distributed to control the flight attitude and position.

2.3. Transformable Mechanism. The transformable process between aerial locomotion and terrestrial locomotion is driven by the servo to rotate 180°, instead of turning over 90°. Figure 5 shows the sequence of the transformable process, taking the transformation from terrestrial locomotion mode to aerial locomotion mode as an example. In the transformable process, in order to avoid the collision between the wheels and the baseplate, the rotational direction of the servo in diagonal direction is the same. The connection between the wheel and the servo is called transformable mechanism and it has a 135° angle (see Figure 6). Reference to the structure of the fast disassembly seat, as shown in Figure 6, the transformable mechanism consist of inter tube, outer tube, and quick-release clip, so the robot has the advantage of

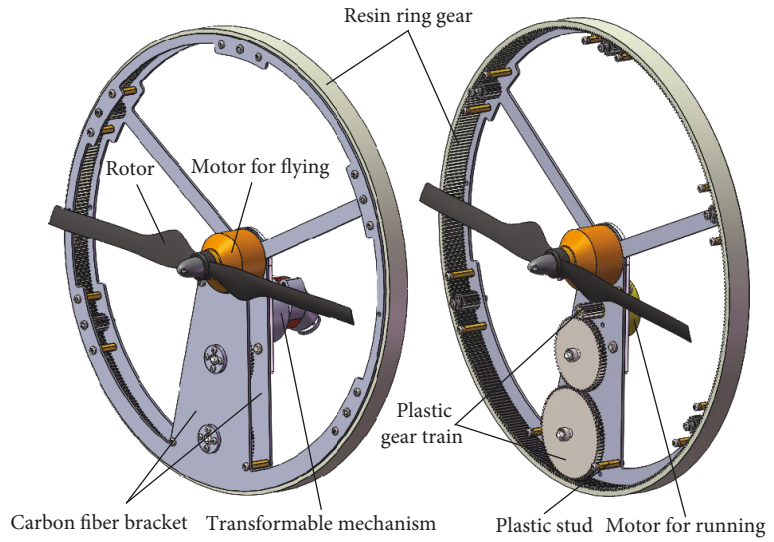

Figure 4: Structure of the driving wheel.

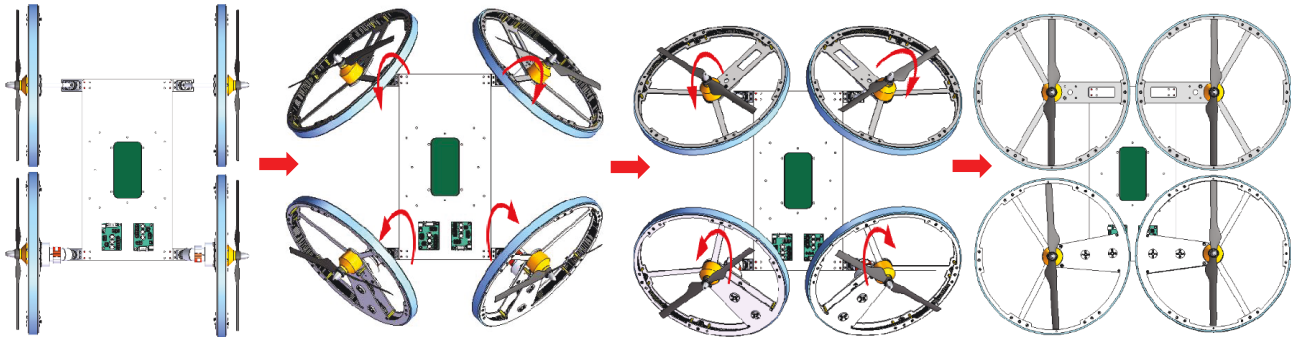

Figure 5: Transformation sequence from terrestrial locomotion mode to aerial locomotion mode.

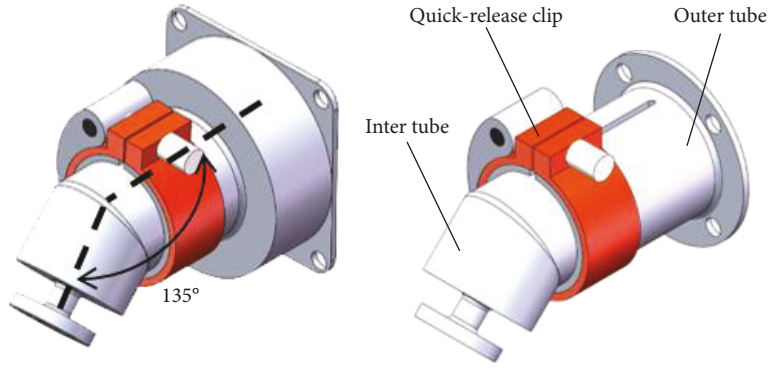

Figure 6: Structure of the transformable mechanism: (a) driving wheel and (b) driven wheel.

portability. The outer tube and motor for running are positioned on the same shaft center.

3. Kinematic and Dynamic Modeling of the Transformable Process

The kinematic and dynamic modeling of aerial locomotion and terrestrial locomotion have been adequately described elsewhere in the literature [19–23]; thus, they are not described in this paper. Because the transformable process of the four wheels is basically the same, here, we only present the transformable process from aerial locomotion mode to terrestrial locomotion mode for the left-rear wheel as an example.

3.1. Kinematic Modeling. Now the research of kinematic modeling is relatively mature [24–26]; to realize the

movement control and verify the kinematic characteristics of the robot, the equivalent angle-axis representation method [27] is used to describe the relationship between the pose of wheel and rotation angle of the servo in the transformable process. In order to express the coordinate system and kinematic parameters of the left-rear wheel more clearly, we simplified the wheel and the transformable mechanism, as shown in Figure 7. The wheel is assumed as the frame {C}, and the transformable mechanism is assumed as a link consists of L_1 and L_2.

According to the rule of equivalent angle-axis representation and right hand, the frame {A} is fixed to the end of the servo shaft and it is considered the reference frame. The frame {B} is described as initially coincident with {A}. The origin of frame {C} is located in the point O, and the pose of wheel is described with the frame {C}. We describe the pose of the wheel in terms of frame {A}. Therefore, the transformable process can be simplified as the frame {C} rotates counterclockwise around the equivalent axis PQ in the Y_aQZ_a plane. In order to get the pose of the frame {C} relative to {A}, the frame {C} is translated to {B} and then {B} rotates counterclockwise around the equivalent axis PQ in the Y_aQZ_a plane.

The translation matrix of the frame {C} relative to frame {B} is given as follows:

$$ {}^{B}_{C}T = \begin{bmatrix} 1 & 0 & 0 & 0 \\ 0 & 1 & 0 & -\frac{\sqrt{2}}{2}L_1 \\ 0 & 0 & 1 & L_2 + \frac{\sqrt{2}}{2}L_1 \\ 0 & 0 & 0 & 1 \end{bmatrix}. \tag{1} $$

The equivalent rotation axis PQ in the Y_aQZ_a plane is given as

$$ \widehat{K} = \begin{bmatrix} 0 & -\frac{\sqrt{2}}{2} & \frac{\sqrt{2}}{2} \end{bmatrix}. \tag{2} $$

The rotation matrix of the frame {B} relative to frame {A} is given as follows:

$$ {}^{A}_{B}T = \begin{bmatrix} \cos\alpha & -\frac{\sqrt{2}}{2}\sin\alpha & -\frac{\sqrt{2}}{2}\sin\alpha & 0 \\ \frac{\sqrt{2}}{2}\sin\alpha & \frac{1}{2}(\cos\alpha+1) & \frac{1}{2}(\cos\alpha-1) & 0 \\ \frac{\sqrt{2}}{2}\sin\alpha & \frac{1}{2}(\cos\alpha-1) & \frac{1}{2}(\cos\alpha+1) & 0 \\ 0 & 0 & 0 & 1 \end{bmatrix}, \tag{3} $$

where α is the rotation angle of the servo shaft in the transformable process; the angular velocity is a constant value.

According to the homogeneous matrix transformation, the pose of the frame {C} relative to frame {A} is given as follows:

$$ {}^{A}_{C}T = {}^{A}_{B}T\,{}^{B}_{C}T = \begin{bmatrix} \cos\alpha & -\frac{\sqrt{2}}{2}\sin\alpha & -\frac{\sqrt{2}}{2}\sin\alpha & -\frac{\sqrt{2}}{2}L_2\sin\alpha \\ \frac{\sqrt{2}}{2}\sin\alpha & \frac{1}{2}(\cos\alpha+1) & \frac{1}{2}(\cos\alpha-1) & -\frac{\sqrt{2}}{2}L_1 + \frac{\cos\alpha-1}{2}L_2 \\ \frac{\sqrt{2}}{2}\sin\alpha & \frac{1}{2}(\cos\alpha-1) & \frac{1}{2}(\cos\alpha+1) & \frac{\sqrt{2}}{2}L_1 + \frac{\cos\alpha+1}{2}L_2 \\ 0 & 0 & 0 & 1 \end{bmatrix}. \tag{4} $$

Equation (4) describes the relationship between the wheel pose and the rotation angle of the servo shaft. Referring to the design model and physical prototype, the parameters are assigned as $L_1 = 36.5$ mm and $L_2 = 66.5$ mm. The wheel was initially in aerial mode. The position and the attitude in the aerial and terrestrial mode of the wheel were drawn in MATLAB, as shown in Figure 8. The direction of the arrow represents the trend of the transformable process.

From the simulation results, the wheel changed from parallel to the ground to perpendicular to the ground; position trajectory was consistent to our expectation. The simulation results confirmed the rationality of the transformable mechanism design and the kinematic modeling.

3.2. Dynamic Modeling. By the force analysis of the left-rear wheel using the isolation method in the transformable process, as shown in Figure 9, we can calculate the servo output torque. In the transformable process, the wheel is not deformed.

According to equation (4), we can get the pose of frame {C} and the position of the point O relative to the

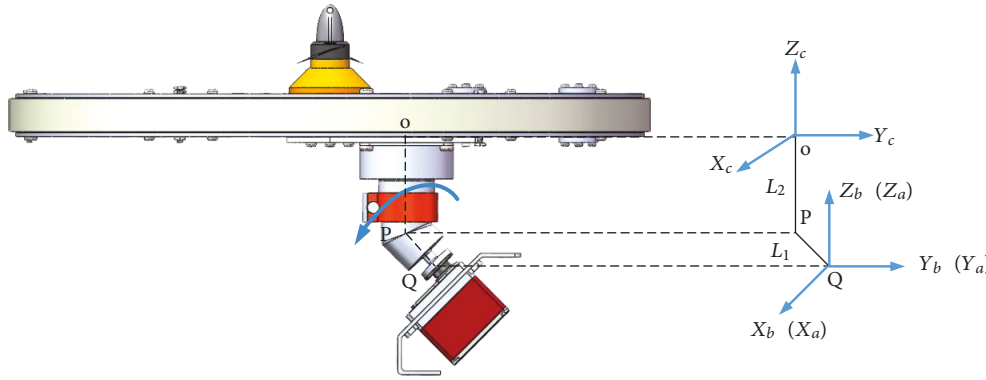

Figure 7: Simplified coordinate model of the wheel and the transformable mechanism.

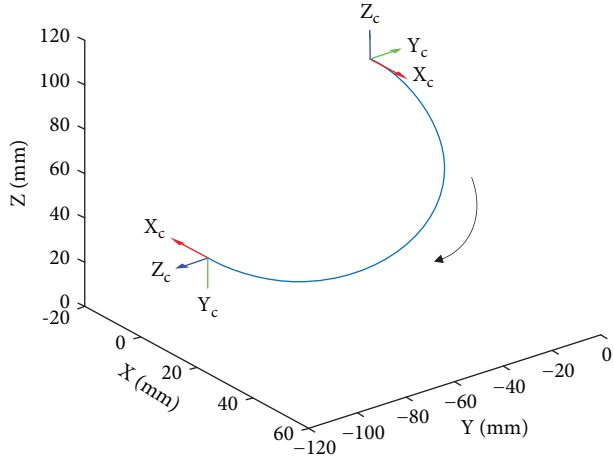

Figure 8: Position and attitude in the aerial and terrestrial mode of the wheel.

frame {A}; the position of the point O in Z_A direction is given as

$$Z_O = \frac{\sqrt{2}}{2}L_1 + \frac{\cos\alpha + 1}{2}L_2. \tag{5}$$

Prototype experiments and design model of the robot show that the wheels contact the ground when the servo axis rotates θ. Then the robot moves along the Z_A direction, and the displacement and acceleration of the robot are given as follows:

$$S = \left(\frac{\sqrt{2}}{2}L_1 + \frac{\cos\alpha + 1}{2}L_2\right) - \left(\frac{\sqrt{2}}{2}L_1 + \frac{\cos\theta + 1}{2}L_2\right)$$
$$= \left(\frac{\cos\alpha}{2} - \frac{\cos\theta}{2}\right)L_2, \tag{6}$$

$$a = \ddot{S}_c = -\frac{L_2}{2}\cos\alpha = -\frac{w^2 L_2}{2}\cos(wt), \tag{7}$$

where w is the angular velocity of the servo shaft. In equation (7), the range of the α is from θ to π.

The direction of the supporting force is opposite to the rotation direction of the gravity, given as

$$F = \frac{G + Ma}{4}, \tag{8}$$

where M is the mass of the robot; a is the acceleration of the robot in the Z_A direction.

The direction of frictional resistance is opposite to the rotation direction of the wheel, given as

$$f = \frac{\mu F}{4}, \tag{9}$$

where μ is the friction coefficient between the resin wheel and the ground.

Figure 10 shows the geometric relationship in the transformable process, which can help us calculate the arm of frictional resistance and supporting force clearly.

The arm of frictional resistance is given as follows:

$$H = h - S,$$
$$L_f = \sqrt{{L_2}^2 + \left(\frac{H}{\sin(\alpha/2)}\right)^2}\sin\left(\frac{3}{4}\pi - ar\tan\frac{H/\sin(\alpha/2)}{L_2}\right), \tag{10}$$

where h is the vertical distance from the point O to the ground in the terrestrial locomotion mode, and its value is 125 mm; $\alpha/2$ is the angle between the wheel and the ground; H is the vertical distance from the point O to the ground.

The arm of the supporting force is given as follows:

$$L_F = X_O + L = X_O + \frac{H}{\tan(\alpha/2)}\cos\frac{\alpha}{2}, \tag{11}$$

where X_O is the position coordinates of point O; L is the vertical distance from point D to point O.

The dynamic analysis of the transformation from terrestrial locomotion mode to aerial locomotion mode is divided into two steps. Next, we calculate the servo output torque referring to the above equations.

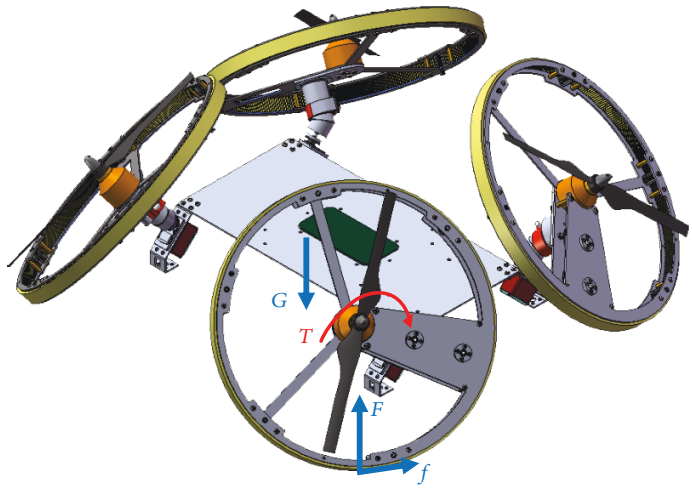

Figure 9: Force analysis of the transformable process.

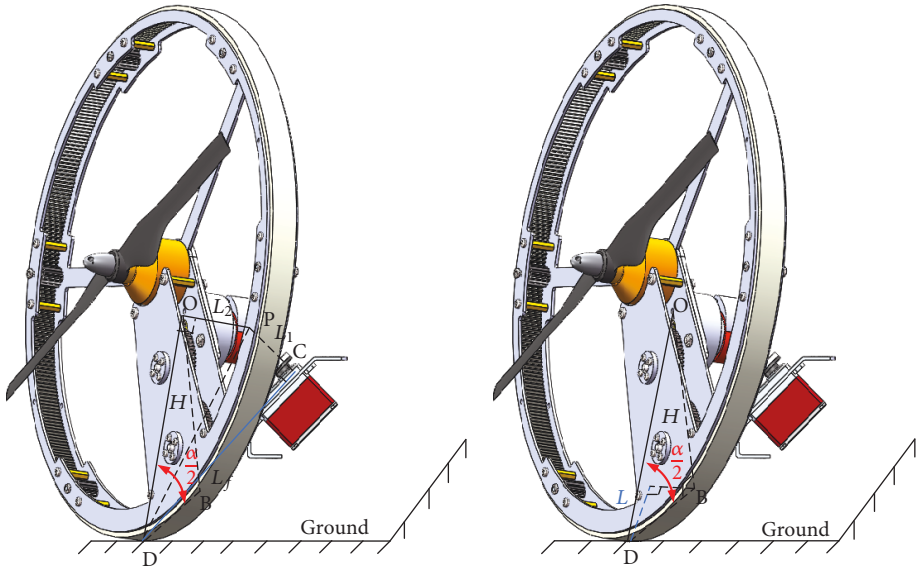

Figure 10: The geometric relationship analysis of a certain angle in the transformable process.

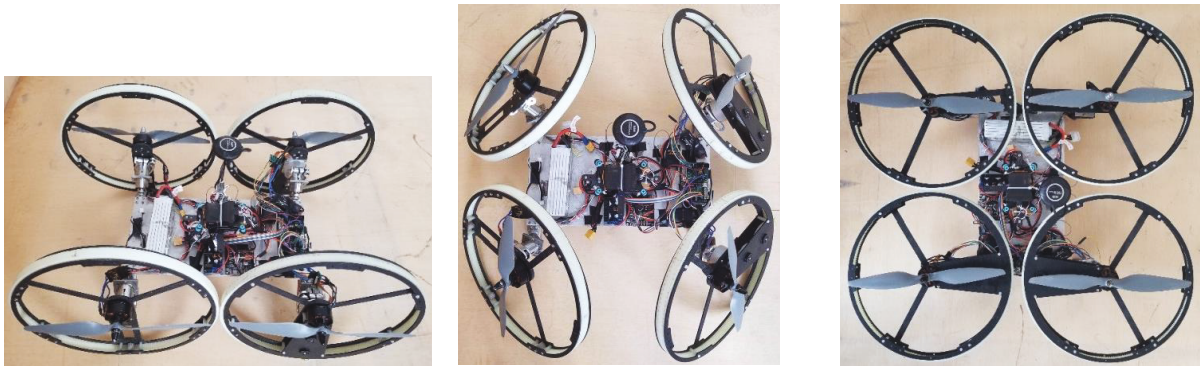

Figure 11: Representations of the physical prototype state: (a) the terrestrial locomotion mode, (b) the state of mode transformation, and (c) the aerial locomotion mode.

Table 1: Prototype dimensions and performance capabilities.

	Terrestrial mode	Aerial mode
Size (mm)	494 × 667 × 328	667 × 667 × 190
Rotor diameter (mm)	304.8	304.8
Wheel diameter (mm)	328	328
Weight (g)	3500	3500
Max velocity (m/s)	1.5	2
Max cargo load (g)	1500	1500
Max flight altitude (m)	\	20

Step 1 is from the aerial locomotion mode to the moment when the wheel contacts the ground. Neglecting the air resistance, the servo only needs to overcome the gravity of the wheel. The output torque is given as follows:

$$l = L_2 \sin \frac{\pi}{4}, \qquad T_1 = mgl \sin \frac{\pi}{4}, \tag{12}$$

where m is the mass of a wheel; l is the arm of gravity of the wheel; g is the gravity vector.

Step 2 is from the wheel contacts the ground to the terrestrial locomotion mode; the servo needs to overcome the gravity of the robot and the frictional resistance. The output torque is given as follows:

$$T_2 = FL_F + fL_f \sin \frac{\pi}{4}. \tag{13}$$

4. Experiments

The performance of the robot was evaluated in both indoor and outdoor environments, you can see in the accompanying video. The terrestrial locomotion and aerial locomotion functions efficiently. Large obstacles can be avoided by flying over or running from the side, and for small obstacles within the obstacle climbing capability, the robot will run straight. Figure 11 shows the physical prototype in terrestrial and aerial modes and the state of mode transformation.

Table 1 shows the dimensions of the physical prototype and the performance capabilities tested in both indoor and outdoor environments.

4.1. Measurement Experiments of Servo Output Torque. In order to measure the output torque of the servo, the experiments about the transformation from aerial locomotion mode to terrestrial locomotion mode were performed with the physical prototype on different terrains including tiled floor, brick, and cement. You can find the experimental data in the accompanying materials. The friction coefficients between the resin wheel and the ground measured by dragging the wheel with a load cell on different terrains are $u_{\text{tiled floor}} = 0.16$, $u_{\text{brick}} = 0.4$, and $u_{\text{cement}} = 0.545$.

According to the above dynamic models, the dynamic simulation results about the output torque were drawn in MATLAB, as shown in Figure 12. The angular velocity of the servo is set as 0.314 rad/s.

From the simulation results, the transformable process was from 0 to 10 s, and it took about 5 seconds when the wheel touched the ground. So we can conclude that the wheel started to touch the ground when the servo shaft rotated about 90 degrees, and the output torque was maximum at this point. The simulation results were helpful for servo selection.

We used digital oscilloscopes to measure and record the current real time, and the servo was powered by a 8.4 V dc power supply. Figure 13 shows the current trend of the four servos on different terrains. In order to compare the experimental results with the theoretical value, the angular velocity of the servo is also set as 0.314 rad/s, and the experiment lasted for 20 s.

According to the working principle of the servo and the relationship between the torque and the current, the output torque is calculated as $T = K_m I$, where K_m is the coefficient of the torque and its value is 2.3 N·m/A. The output torque tendencies of a single servo are shown in Figure 14.

Comparing Figures 12 and 14, the experimental results have the same tendency with the dynamic simulation result, but there are some deviations between them. (1) The experimental results indicate the output torque of the servo is larger than what is predicted from theoretical analysis. We attribute this mostly to the uneven ground that are not modeled, and the servo efficiency is reduced due to long-term use. (2) The experimental results show that there is a longer adjustment time before the torque of the servo reaches its maximum value. According to the experiments, the time from about the fifth second to the maximum current value is the adjustment time of servo, the pose of the wheel did not change during this period. Future research will investigate these effects in the modeling process and optimize the current loop of the servo to speed up its response speed.

4.2. Energy Analysis. In order to compare the energy consumption in its terrestrial and aerial locomotion modes, we calculated the operating time and distance of the robot by measuring the current using the wireless galvanometer when the robot is moving at a constant speed.

Table 2 shows the experimental data, and Table 3 shows the calculated value of the operating time and distance. The weight of the prototype was 3.5 kg, and it was weighted to 4.2 kg in the experiment.

The experimental results show that with the same battery the robot can fly about 23040 s and travels 34560 m and it can run 698 s and travels 1396 m. Therefore, the operating time increased about 33 times in the terrestrial mode, and the distance is still 25 times greater comparing to the aerial mode. Our robot takes account of the operating time and distance.

5. Conclusions

In this paper, we designed a novel transformable robot that is capable of terrestrial locomotion and aerial locomotion and enables to transform between the two modes at will for

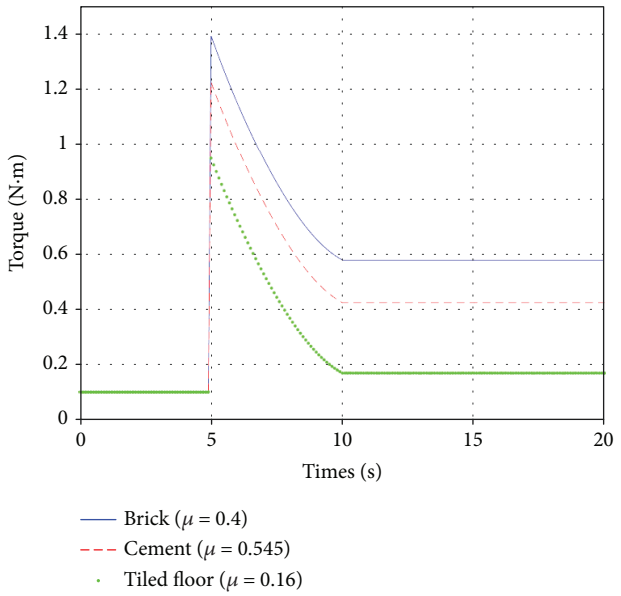

Figure 12: The dynamic simulation results of the output torque in the transformable process.

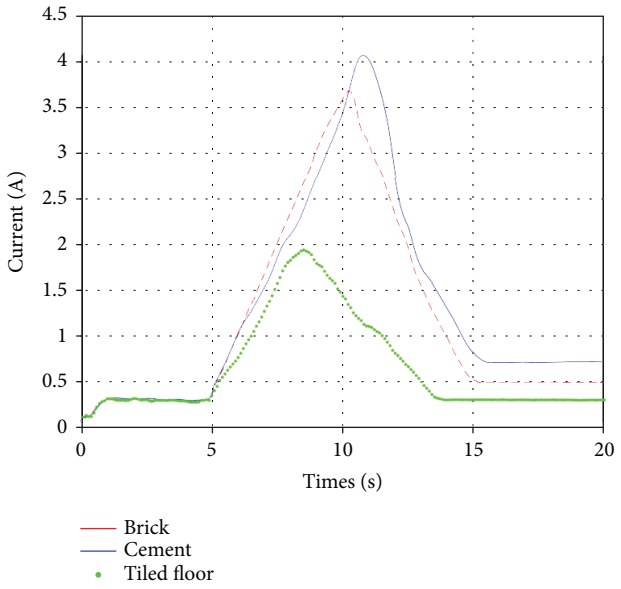

Figure 13: Experimental current tendencies of the four servos on different terrains.

overcoming obstacles. Firstly, we explained the outline of the platform and focus on analyzing the design of the driving wheel and transformable mechanism. Then, the kinematic and dynamic models about the transformable process were accurately established, which can provide an important reference to the key parameters design. Finally, a series of experiments about the running, mode transformation, and flying in both indoor and outdoor environments are performed. The experimental results show that the terrestrial locomotion and aerial locomotion function efficiently, and obstacles can be overcomed by flying over or running from the side. Moreover, the transformable experiments confirmed the validity

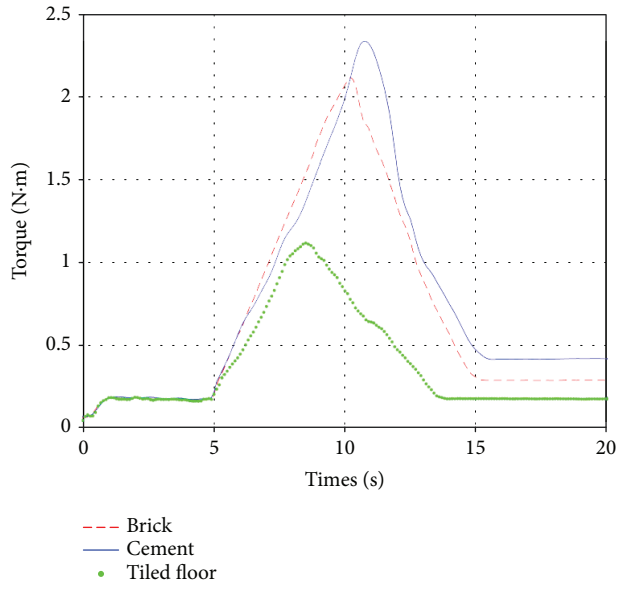

Figure 14: Calculated the output torque tendencies of a single servo.

Table 2: Experimental data in aerial and terrestrial modes.

	Terrestrial mode	Aerial mode
Current (A)	0.5	16.5
Discharge capacity (mAh)	3200	3200
Velocity (m/s)	1.5	2

Table 3: Calculated data of operating time and distance.

	Terrestrial mode	Aerial mode
Operating time (s)	23040	698
Operating distance (m)	34560	1396

of the kinematic and dynamic models that are important to transformable mechanism design and servo selection. The robot in the terrestrial mode can travel a distance almost 25 times greater and operate about 33 times longer compared to the aerial mode. The robot has a longer operating time and good mobility.

Design optimization is a constant issue and requires a significant attention. In the future, we plan to optimize the transformable mechanism and the current loop of the servo to speed up its response speed, making the transformable process between aerial locomotion mode and terrestrial locomotion mode smoother and more stable. The ongoing research also continues to reduce the weight of the robot and improve both running and flying performance.

Data Availability

The experimental data used to support the findings of this study can be available at https://github.com/WangHeHe008/Supplementary-Materials.git.

Conflicts of Interest

The authors declare that there is no conflict of interest regarding the publication of this paper.

Acknowledgments

This research work is supported by the Defense Industrial Technology Development Program (JCKY2017602C016).

Supplementary Materials

Supplementary Materials contain a video about the terrestrial locomotion, aerial locomotion, transformation between the two modes, and obstacle climbing. Besides, the experimental data are the current changes of four servos measured by digital oscilloscope in a transformable process. *(Supplementary Materials)*

References

[1] T. H. Chung, G. A. Hollinger, and V. Isler, "Search and pursuit-evasion in mobile robotics: a survey," *Autonomous Robots*, vol. 31, no. 4, pp. 299–316, 2011.

[2] S. Tadokoro, *Rescue Robotics: DDT Project on Robots and Systems for Urban Search and Rescue*, Springer Verlag, 2009.

[3] H. Tennekes and H. Tennekes, *The Simple Science of Flight: From Insects to Jumbo Jets*, The MIT Press, 2009.

[4] D. Lentink and M. H. Dickinson, "Biofluiddynamic scaling of flapping, spinning and translating fins and wings," *Journal of Experimental Biology*, vol. 212, no. 16, pp. 2691–2704, 2009.

[5] Q. Yang, J. Yu, M. Tan, and W. Wang, "Preliminary development of a biomimetic amphibious robot capable of multi-mode motion," in *2007 IEEE International Conference on Robotics and Biomimetics (ROBIO)*, pp. 769–774, Sanya, China, December 2007.

[6] J. W. Yeol and C.-H. Lin, "Development of multi-tentacle micro air vehicle," in *2014 International Conference on Unmanned Aircraft Systems (ICUAS)*, pp. 815–820, Orlando, FL, USA, May 2014.

[7] M. Kovac, J. Zufferey, and D. Floreano, *Towards a Self-Deploying and Gliding Robot*, Flying insects and robots, 2009.

[8] K. Peterson and R. Fearing, "Experimental dynamics of wing assisted running for a bipedal ornithopter," in *2011 IEEE/RSJ International Conference on Intelligent Robots and Systems*, pp. 5080–5086, San Francisco, CA, USA, September 2011.

[9] R. J. Bachmann, F. J. Boria, R. Vaidyanathan, P. G. Ifju, and R. D. Quinn, "A biologically inspired micro-vehicle capable of aerial and terrestrial locomotion," *Mechanism and Machine Theory*, vol. 44, no. 3, pp. 513–526, 2009.

[10] C. J. Pratt and K. K. Leang, "Dynamic underactuated flying-walking (DUCK) robot," in *2016 IEEE International Conference on Robotics and Automation (ICRA)*, pp. 3267–3274, Stockholm, Sweden, May 2013.

[11] A. Kalantari and M. Spenko, "Design and prototyping of a walking quadrotor," in *ASME 2012 International Design Engineering Technical Conferences and Computers and Information in Engineering Conference*, Chicago, IL, USA, August 2012.

[12] A. Kalantari and M. Spenko, "Design and experimental validation of HyTAQ, a hybrid terrestrial and aerial quadrotor," in *2013 IEEE International Conference on Robotics and Automation*, pp. 4445–4450, Karlsruhe, Germany, May 2013.

[13] A. Kalantari and M. Spenko, "Modeling and performance assessment of the HyTAQ, a hybrid terrestrial/aerial quadrotor," *IEEE Transactions on Robotics*, vol. 30, no. 5, pp. 1278–1285, 2014.

[14] A. Kossett, J. Purvey, and N. Papanikolopoulos, "More than meets the eye: a hybrid-locomotion robot with rotary flight and wheel modes," in *2009 IEEE/RSJ International Conference on Intelligent Robots and Systems*, St. Louis, MO, USA, October 2009.

[15] A. Kossett, R. D'Sa, J. Purvey, and N. Papanikolopoulos, "Design of an improved land/air miniature robot," in *2010 IEEE International Conference on Robotics and Automation*, pp. 632–637, Anchorage, AK, USA, May 2010.

[16] A. Kossett and N. Papanikolopoulos, "A robust miniature robot design for land/air hybrid locomotion," in *2011 IEEE International Conference on Robotics and Automation*, pp. 4595–4600, Shanghai, China, May 2011.

[17] L. Daler, J. Lecoeur, P. B. Hahlen, and D. Floreano, "A flying robot with adaptive morphology for multi-modal locomotion," in *2013 IEEE/RSJ International Conference on Intelligent Robots and Systems*, pp. 1361–1366, Tokyo, Japan, November 2013.

[18] R. Quinn, D. Kingsley, J. Offi, and R. Ritzmann, "It has got whegs," in *2002 IEEE International Conference on Robotics and Automation (ICRA02) Video Proceedings*, Washington, DC, USA, 2002.

[19] H. Zhu, J. Shi, J. Wang, and J. Ma, *Terrestrial Locomotion and Control Technique of Miniature Land-Air Hybrid robot*, Beijing Institute of Technology, 2015.

[20] D. Mellinger, M. Shomin, and V. Kumar, "Control of quadrotors for robust perching and landing," in *Proceeding of the 2010 International Powered Lift Conference*, pp. 1203–1225, Philadelphia, PA, USA, October 2010.

[21] H. Huang, G. Hoffmann, S. Waslander, and C. Tomlin, "Aerodynamics and control of autonomous quadrotor helicopters in aggressive maneuvering," in *2009 IEEE International Conference on Robotics and Automation*, pp. 3277–3282, Kobe, Japan, May 2009.

[22] P. Martin and E. Salaun, "The true role of accelerometer feedback in quadrotor control," in *2010 IEEE International Conference on Robotics and Automation*, pp. 1623–1629, Anchorage, AK, USA, May 2010.

[23] S. Omari, M.-D. Hua, G. Ducard, and T. Hamel, "Nonlinear control of VTOL UAVs incorporating flapping dynamics," in *2013 IEEE/RSJ International Conference on Intelligent Robots and Systems*, pp. 2419–2425, Tokyo, Japan, November 2013.

[24] Y. Zhang and J. Jiang, "Kinematics analysis and simulation study of an archwire bending robot," *Chinese High Technology Letters*, vol. 22, no. 7, pp. 727–734, 2012.

[25] Q. He, H. Kang, J. Zhu, and Y. Xu, "Dynamic mechanical properties of working device of rotary drilling rig under lift-arm luffing conditions," *Journal of Central South University of Science and Technology*, vol. 43, no. 6, pp. 2150–2156, 2012.

[26] J. Luo and G. Hu, "Study on the simulation of robot motion based on MATLAB," *Journal of Xiamen University Natural Science*, vol. 44, no. 5, pp. 640–644, 2005.

[27] J. J. Craig, *Introduction to Robotics: Mechanics and Control*, Pearson Education Inc, 2005.